



Multilevel analysis of six species of *Phyllostachys* bamboo and *Arundo donax*: preliminary survey on Italian grown stands

Silvia Greco¹ · Luisa Molari¹ · Giovanni Valdrè² · Jose Jaime Garcia³

Received: 11 September 2023 / Accepted: 21 March 2024
© The Author(s) 2024

Abstract

The paper focuses on a multilevel analysis considering six species of bamboo of the *Phyllostachys* family (*P. bambusoides*, *edulis*, *iridescens*, *viridiglaucescens*, *violacescens*, and *vivax*) and *Arundo donax* grown in temperate climates, most of them not already studied in the literature. The analysis is divided into three levels. The analysis at the first level (the microscopic scale) includes an anatomical study to assess the shapes and dimensions of the vascular bundles and the sclerenchymatic and parenchymatic tissues. At the second mesoscale level, the percentage and distribution of the fibres, voids and parenchyma are calculated. At the third level, the macroscopic one, a discussion of the influence of the microscopical properties on mechanical properties is carried out. Despite the limited number of specimens analysed at the microscale level, differences between species emerged from the analysis and influenced the macroscopic characteristic values. In particular, the morphology of the components differs, especially in the case of *Arundo donax*, which presents a unique distribution of its components along the culm wall. Different contents of each component are observed for the species analysed. Moreover, an innovative analysis that focuses on the presence and distribution of voids is presented, which have a fundamental role in the mechanical behaviour of this material. The analysis did not account for the influence of the environment on composition or anatomical and physical characteristics.

✉ Luisa Molari
luisa.molari@unibo.it

¹ DICAM, Alma Mater Studiorum – Università di Bologna, Bologna, Italy

² BIGEA, Alma Mater Studiorum – Università di Bologna, Bologna, Italy

³ Escuela de Ingeniería Civil y Geomática - Universidad del Valle, Cali, Colombia

Introduction

The utilization of locally sourced natural materials holds great promise for the building industry due to their sustainable production, transportation, and disposal. Among these materials, bamboo and *Arundo donax* exhibit a unique combination of high mechanical resistance, low specific weight, and a rapid growth rate, making them viable substitutes for environmentally harmful materials in various applications (Zea and Habert 2014). However, the natural origin of these plants gives rise to variations in composition as well as anatomical and physical characteristics, which significantly impact their durability and strength (Liese and Köhl 2015). Understanding the relationship between their microstructure and mechanical behaviour presents a challenge due to their heterogeneous composition.

Bamboo, unlike wood, does not exhibit secondary thickening growth, which hinders its geometric adaptation to mechanical stresses. This absence enhanced the structural optimization at the material level (Wang et al. 2012). Bamboo has been recognized as a functionally graded composite material (Amada et al. 1997) due to its multi-component structure and arrangement. Its cribro-vascular vessels, responsible for transporting water and nutrients, extend from the internal to the external part of the culm wall, increasing in number while decreasing in diameter. The distribution and morphology of vessels and vascular bundles vary significantly within the culm. Previous investigations by Dai et al. (2023) provided insights into the morphological characteristics of the vascular bundles of *Dendrocalamus sinicus*, describing their length, width, length-to-width ratio, and area using quadratic functions. Li et al. (2007) explored the concentration of vascular bundles and discovered notable differences between the bottom and top parts of the culm, as well as between the outer and inner sections of the culm wall. Some studies also indicate a relationship between the number of vascular bundles and mechanical characteristics (Wahab et al. 2012).

The sclerenchymatous tissue surrounding the vessels consists of longitudinally developed fibre cells, which have an almost hexagonal cross-section of different dimensions. These cells provide mechanical support and contribute to the remarkable mechanical properties of bamboo, as extensively studied by Liu et al. (2012), Wang et al. (2013), Krause et al. (2016) and Dessalegn and Singh (2019). The fibre cells possess a strongly thickened secondary wall with a microfibril percentage higher than the matrix. The structure is characterized by alternating lamellae with different fibril orientations, enabling the cells to withstand internal stress and facilitate longitudinal expansion (Parameswaran and Liese 1976). Additionally, the fibre cells undergo lignification improving the strength and stiffness of the plant.

The vascular bundle is embedded in the parenchymatous tissue which is made of elongated cells, each composed of the middle lamella, primary wall and cytoplasmic structure. This type of cell only has a thin cell wall made of microfibrils embedded in a large quantity of matrix made of water and pectins. Parenchymatic tissue is not subjected to the lignification process for bamboo.

Similarly, *Arundo donax* shares many components with bamboo but exhibits a different arrangement. Spatz et al. (1997) described a ring of sclerenchymatous

fibres with small vascular bundles surrounded by a layer of the cortical parenchyma on the external part of the culm wall, while the inner parenchymatous tissue contained numerous vascular bundles with sclerenchymatous bundle sheaths. Previous studies by Spatz et al. (1997) and Rüggeberg et al. (2010), have investigated the role of different components in the mechanical behaviour of *Arundo donax*. Notably, parenchymatous cells in *Arundo donax* possess significantly lignified cell walls, in contrast with bamboo parenchymatous cells.

While bamboo has been extensively studied (Fangchun 1981; Janssen 1991; Trujillo 2016), the current knowledge is primarily limited to certain Asian and South American species. *Phyllostachys* is a widely recognized bamboo family, particularly in temperate climates such as Europe (Liese and Köhl 2015). However, detailed information crucial for accurately grading bamboo and using appropriately each species of this big family is present only for *edulis*, but they are still lacking for the other species.

In turn, *Arundo donax*, native to Mediterranean areas, has recently regained attention as an inexpensive and sustainable construction material. Numerous studies (Spatz et al. 1997; Conte et al. 2018; Hardion et al. 2014; Molari et al. 2021) have explored its potential for various applications, such as vibrating reeds for woodwind instruments or as a source of biomass.

In this study, we analyse and compare six types of *Phyllostachys* species and *Arundo donax*. The analysis is performed at three different levels. The first level focuses on microscopic analysis to describe the components: the vascular bundles, the sclerenchymatic and parenchymatic tissues and cells. Given the intricate and time-intensive nature of specimen preparation, this microscopic study is conducted on two samples for each species, corresponding to two different longitudinal locations along the culm length.

The second part examines the content and distribution of these components, including the density distribution of the voids, which is not generally analysed even if it is crucial to understand the mechanisms of bamboo failure under transverse loading (Greco et al 2022). In the last level, a discussion on the relation between the obtained data and the macroscopic characteristic is carried out and the data are used to predict some of the macroscopic mechanical properties obtained in previous studies by the authors (Greco et al. 2019, 2023; Molari and García (2021); Molari et al. 2020).

Materials

All the specimens used in this study were obtained from untreated culms of bamboo and *Arundo donax*. Six species of the *Phyllostachys* Genus (Poaceae family) were evaluated: *P. edulis*, *P. bambusoides*, *P. viridiglaucescens*, *P. vivax*, *P. violacescens* and *P. iridescens*. In particular, *P. bambusoides*, *P. iridescens*, and *P. vivax* are from Langhe (Piemonte region, North-West of Italy), *P. edulis* is from Pordenone, (Friuli Venezia Giulia, North-East of Italy), *P. viridiglaucescens* is from Selvaiana Capez-zano Pianore (Tuscany, central Italy) and *P. violacescens* is from Bologna (Emilia Romagna, central part of Italy). *Arundo donax* was cultivated in Cadriano, a small

town close to Bologna. All the bamboo culms were between three and four years old, and they were collected in the winter of 2018 and were stored in a protected warehouse at the University of Bologna. For each species, six different culms with the geometrical characteristics reported in Table 1 were chosen. We examined two distinct sections from each culm of bamboo and *Arundo donax*: the upper section (part A) was taken from 2.5 to 3.5 m above the ground, and the lower section (part B) was taken from 0.5 to 1.5 m above the ground. These six culms per species underwent mechanical testing, as detailed in published studies (Molari et al. 2020; Greco et al. 2019), whose results were considered for the macroscopic analysis level presented in the last part of this paper. For microscopic analysis, we selected one culm that displayed average geometrical characteristics. From this culm, we prepared one sample from each part of the culm (A and B). The choice to limit our microscopic sample size was due to the intensive and time-consuming nature of the analysis process. Although this sample size is a recognized limitation of our analysis, other studies cited by Liese and Schmitt (2006), have found consistent microstructures in multiple culm samples, while others acknowledge variations.

Anatomic analysis

Both reflected and transmission-polarized optical microscopy analyses were performed to observe the microstructure of the material. For polarized optical microscopy (POM), thin sections (about $30 \pm 1 \mu\text{m}$) of each bamboo sample were prepared, and polished at least with $0.5 \mu\text{m}$ grit over areas several mm^2 in size. Both analyses were performed on thin sections, employing a Zeiss Photomicroscope III with polarized light and digitized with an Edmund Optics CMOS-sensor colour camera.

Table 1 Mean values of diameter (D) and thickness (d) in the portion of the culms used in this study of the culms examined for the different species (Molari et al. 2020)

Species		D (mm)		d (mm)		n. culms
		Mean	SD	Mean	SD	
<i>P. bambusoides</i>	A	58.1	3.2	4.7	0.5	6
	B	58.7	3.0	5.9	0.4	6
<i>P. edulis</i>	A	62.4	3.9	5.8	0.6	6
	B	71.8	0.8	8.7	0.8	6
<i>P. iridescens</i>	A	61.7	2.3	5.7	0.3	6
	B	62.1	3.2	7.8	1.1	6
<i>P. violacescens</i>	A	46.2	4.1	3.9	0.2	6
	B	56.1	3.3	5.1	0.3	6
<i>P. viridiglaucescens</i>	A	55.4	3.7	5.8	1.0	6
	B	61.5	2.9	7.0	1.3	6
<i>P. vivax</i>	A	77.7	8.9	5.5	0.8	6
	B	81.2	6.7	7.1	0.4	6
<i>Arundo donax</i>	A	10.3	0.04	1.5	0.11	9
	B	21.8	0.06	3.8	0.14	12

A small portion of the bamboo wall was cut using a circular saw for each species in the two parts of the culm previously described as Parts A and B.

The preparation of the thin bamboo sections (about $30 \pm 1 \mu\text{m}$) required the use of embedding and surface impregnation techniques. Samples were embedded in a vacuum with resin to provide a robust supporting layer. The type of resin is an epoxy resin (Hardrock 554) with a specific hardener, produced by REMET SAS (Casalecchio di Reno, Bologna, Italy). Then, the preparation of thin sections included the creation of a flat surface ($\pm 1 \mu\text{m}$) with abrasives. After this procedure, a glass slide was glued onto that surface, and finally, the specimens were thinned down to $30 \mu\text{m}$ using cutting, lapping and polishing (at least with $0.5 \mu\text{m}$ grit), over areas several mm^2 in size.

Different zooms were used: 2.5X, 10X, 25X and 40X, to analyse microstructural details at various magnifications. An image from the top and one from the bottom of each species were selected.

Vascular bundles: disposition, dimension, and shape

The disposition of bamboo and *Arundo donax* components along the culm wall is shown in Fig. 1a, b respectively.

The culm tissues have an organization that can maximize their mechanical strengths. The mechanical stability of the culms depends on the correct insertion of the rigid sheaths of fibres supporting the vascular bundles in the soft and compressible matrix of parenchyma, consisting of thin-walled cells that do not contribute to the stiffness of the culms. Also, the orientation of the vascular bundle influences the mechanical characteristics (Kanzawa et al. 2011).

In the case of bamboo (Fig. 1a), the increase of sclerenchymatous sheaths is evident from the inner to the outer part of the culm wall, in parallel with the reduction of the area occupied by parenchyma. In the case of *Arundo donax* (Fig. 1b), two zones are distinguishable: the inner one, in which vascular bundles are rather homogeneously embedded in the ground parenchyma, and the second, in the neighbourhood of the outer culm wall, in which the ring of sclerenchymatic tissue divides the cortical parenchyma from the rest of the section.

The components of a bamboo vascular bundle are clearly visible in Fig. 2a. They are a group of small phloematic vessels, two big xilematic vessels, and an intercellular space that is a cavity derived from an ancient proto-xilematic vessel, all of which are protected by four sclerenchyma sheaths, embedded in the ground parenchyma. According to Grosser and Liese (1971) classification, in *P. edulis*, *P. bambusoides*, *P. iridescens*, *P. violascens*, *P. vivax* and *P. viridiglaucens*, there is only one type of vascular bundle along the wall thickness, as there is for all species with leptomorph rhizomes, in which there is only a central vascular strand, and the island is concentrated only in sheaths around vessels. The shape of the sheaths varies along the thickness, as reported in Table 2. The sheaths appear as four little islands around the vessels and the intercellular space, on the inner side, while they start stretching towards the external side, where only two big fibre islands surround the vessels: a bigger one for the two xilematic vessels and a smaller one for the phloematic ones.

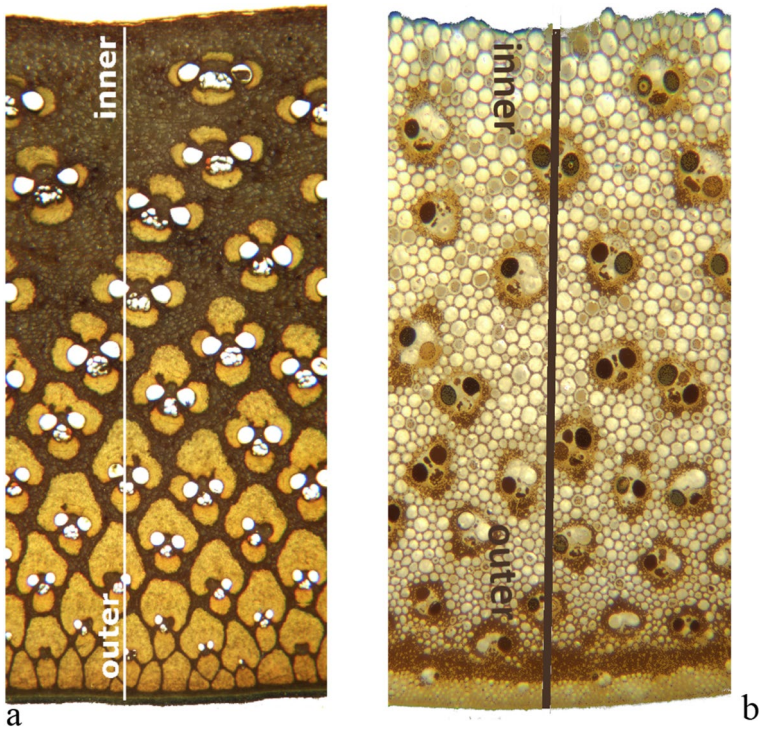


Fig. 1 Cross-section of a culm wall of a *P. iridescens* (a) and of an *Arundo donax* (b), with the inner side on the top part of the pictures, and the external side on the bottom part of the pictures. Transmission optical microscope, enlargement 2.5×

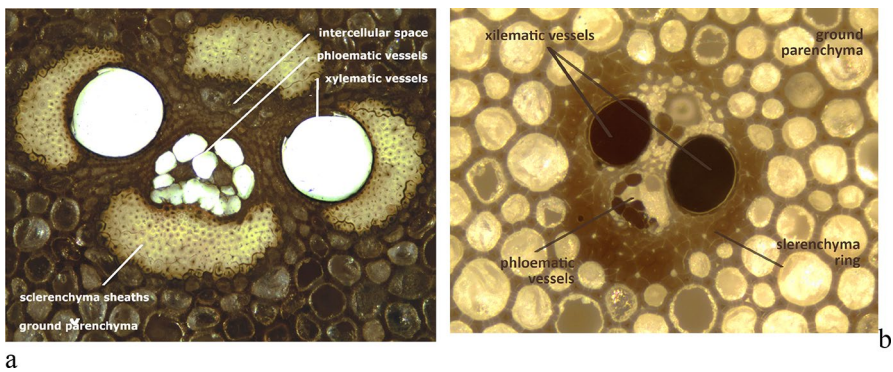


Fig. 2 Vascular bundle from the inner side of the wall from part A of the culm of a *Phyllostachys viridiglaucescens* (a) and from the middle part of the wall from part B of the culm of *Arundo donax* (b). Transmission optical microscope, enlargement 10×

Table 2 A vascular bundle was taken from the inner, middle and outer positions along the culm wall, for part A (2.5–3.5 from the ground) and part B (0.5–1.5 m from the ground) of each culm

	INNER		MIDDLE		OUTER	
	Part A	Part B	Part A	Part B	Part A	Part B
<i>P. bambusoides</i>						
<i>P. edulis</i>						
<i>P. iridescens</i>						
<i>P. violacescens</i>						
<i>P. vivax</i>						
<i>P. viridiglaucescens</i>						
<i>Arundo donax</i>						

Transmission optical microscope, enlargement 10×

The intercellular spaces seem to disappear. No differences were found in terms of shapes between the six species, while the proportion between fibre sheaths and vessels changes visibly, as will be discussed below. As a result, the inner vascular bundle has a greater width and a smaller height, while the outer vascular bundle has a greater height and a smaller width. The dimensions of an average vascular bundle are reported in Table 3. Generally, vascular bundles from the top part of the culm look smaller than those from the bottom part, both in width and height. The trend is the same for the vascular bundles in the external part compared to the inner one. Different species present similar dimensions of the vascular bundles, except for *P. violacescens* species, which has lower vascular bundle dimensions, both in height and width.

Table 3 Dimensions of an average vascular bundle from the inner, middle, and outer parts of the culm wall considering three typical bundles in each portion

	Inner			Middle			Outer			
	W_{\max} (mm)	H_{\max} (mm)	H/W	W_{\max} (mm)	H_{\max} (mm)	H/W	W_{\max} (mm)	H_{\max} (mm)	H/W	
<i>P. bambusoides</i>	A	0.68	0.41	0.60	0.46	0.63	1.37	0.25	0.42	1.68
	B	0.72	0.48	0.67	0.49	0.58	1.18	0.25	0.49	1.96
<i>P. edulis</i>	A	0.66	0.40	0.61	0.49	0.47	0.96	0.31	0.51	1.65
	B	0.72	0.45	0.63	0.59	0.57	0.97	0.35	0.49	1.40
<i>P. iridescens</i>	A	0.42	0.36	0.86	0.37	0.41	1.11	0.24	0.40	1.67
	B	0.45	0.37	0.82	0.41	0.45	1.10	0.28	0.40	1.43
<i>P. violascens</i>	A	0.66	0.47	0.71	0.56	0.56	1.00	0.32	0.59	1.84
	B	0.75	0.51	0.68	0.58	0.65	1.12	0.40	0.66	1.65
<i>P. vivax</i>	A	0.70	0.40	0.57	0.54	0.59	1.09	0.36	0.56	1.56
	B	0.75	0.44	0.59	0.60	0.72	1.20	0.34	0.49	1.44
<i>P. viridiglaucescens</i>	A	0.76	0.50	0.66	0.58	0.61	1.05	0.34	0.60	1.76
	B	0.76	0.53	0.70	0.51	0.69	1.35	0.30	0.57	1.90
<i>Arundo donax</i>	A	0.27	0.30	1.11	0.24	0.19	0.79	0.19	0.15	0.79
	B	0.20	0.33	1.65	0.21	0.21	1.00	0.18	0.18	1.00

W stands for the width (measured along the circumferential direction), H for the height (measured along the radial direction) of the vascular bundle, and A and B indicate the position along the culm

A vascular bundle of *Arundo donax* is illustrated in Fig. 2b. Its composition is the same as that of the bamboo vascular bundle, but there is no subdivision into islands of fibres as in bamboo. A ring of sclerenchymatous tissue surrounds the vessels, and the part around the phloematic vessels is thicker. Small parenchymal cells are present between the vessels, while the ground parenchyma surrounds the entire bundle. Some other vessels are present between the outer part of the sclerenchymatous ring and the ground parenchyma. No difference in the shape of the vascular bundles was found along the thickness, as visible in Table 2. The dimensions of the vascular bundles decrease appreciably near the external part of the culm wall, as noticed in Table 3. Moreover, it was found that vascular bundles from the upper part of the culm (part A) are smaller than those of the lower part (part B).

The ratio of height to width (H/W) does not show consistent differences between sections A and B of the culms, which are at varying heights (Table 3).

This suggests that variability within the stem is less significant than that between stems. In contrast, the ratio H/W consistently increases from the inner to the outer portions of the culm wall. In particular, the range for all species is 0.57–0.86 in the inner material and 1.40–1.96 in the outer material, which compares well to values around 0.7–1.0 for the inner material and 1.2–1.7 for the outer material, as reported in Kanzawa et al. (2011). The trend with height for *Arundo donax* appears to be different since the ratios H/W on the inner are higher than those at the outer position.

Sclerenchymatic cells: dimensions and shape

The sclerenchymatic tissue was observed using the optical transmission technique. In this case, the lumen of the fibre behaves as a channel through which the light goes and appears white in the reported picture. The reflection technique was not used because the image appears poorly defined.

Fibre dimensions vary with respect to age, position along the culm, and location within the culm wall. The microstructure can also be affected by environmental traits. As the culm develops, new layers of secondary cell wall are deposited within the support fibers, resulting in increased cell wall thickness and cellular luminal reduction (Gritsch et al. 2004; Murphy and Alvin 1997). Measurements for a mean fibre are reported in Table 4 for every species of the inner and outer parts of the culm. The average fibre diameter is in the range of 12–20 μm and 15–22 μm for the inner and outer positions, respectively.

The values are similar to those reported in the literature. For a *Gigantochloa scortechinii*, Wahaba et al. (2012) report a dimension of 18.49 μm in the outer part and 19.56 μm in the inner part, and for a *Guadua angustifolia* Osorio et al. (2018) show results in the range from 10 to 25 μm .

The average lumen diameter ranges from 2 to 6 and from 2 to 7 μm for the internal part and the external parts, respectively. The dimensions are consistent with those found in the literature. For example, Jiang (2016) measured 2.35 μm for *P. glauca*, while Wahab et al. (2012) reported that the dimensions for *G. scortechinii* ranged from 5.44 μm in the outer part to 5.96 μm in the inner part.

Table 4 Fibre morphology

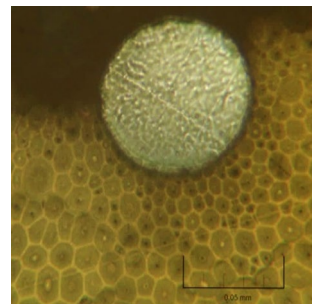
	Inner			Outer			
	Fibre diameter (μm)	Lumen diameter (μm)	Wall thickness (μm)	Fibre diameter (μm)	Lumen diameter (μm)	Wall thickness (μm)	
<i>P. bambusoides</i>	A	18	4.0	7.0	20	4.0	8.0
	B	16	2.8	6.6	22	7.0	7.5
<i>P. edulis</i>	A	14	2.0	6.0	17	3.5	6.8
	B	14	3.0	5.5	15	2.0	6.5
<i>P. violacescens</i>	A	12	3.0	4.5	17	3.8	6.6
	B	13	4.0	4.5	15	3.0	6.0
<i>P. viridiglaucescens</i>	A	15	3.0	6.0	21	4.0	8.5
	B	14	4.0	5.0	19	4.0	7.5
<i>P. iridescens</i>	A	16	2.0	7.0	21	3.0	9.0
	B	18	6.0	6.0	17	2.5	7.3
<i>P. vivax</i>	A	20	6.0	7.0	19	2.0	8.5
	B	13	2.0	5.5	21	5.8	7.6
<i>Arundo donax</i>	A	14	2.0	6.0	16	1.5	7.2
	B	18	1.0	8.5	20	3.0	8.5

Fibre diameters, lumen diameters, and cell wall thickness are here reported for parts A (2.5–3.5 m from the ground) and B (0.5–1.5 m from the ground) of all six bamboo species. The data refer to the average dimension of the fibres considering three typical bundles in each portion. While no information is currently available for the variability in this study, published papers (Khantayanuwong et al. 2023; Hartono et al. 2022) have recorded standard deviations of 10% for fibre diameter and wall thickness and 30% for lumen diameter

Cell wall thickness goes from 4.5 to 7 μm and from 6 to 9 μm for the internal or external cells, resulting in very different results in these two cases. These values are similar to those reported in the literature. Jiang (2016) measured 3.72 μm for *P. glauca*, while Wahab et al. (2012) observed that the dimensions for *G. scortechinii* ranged from 7.03 μm in the outer part to 6.8 μm in the inner part.

The ratio between the dimension of the entire cell and its wall thickness is almost constant. Fibres of the same vascular bundles can change in dimension, as shown

Fig. 3 Progressive increase of fibre dimension from the vessel's edge to the parenchymatic matrix. An image of a *P. edulis* from the upper part of the culm. Transmission optical microscope, 25 \times enlargement



in Fig. 3. The cross-sectional dimension of the bundles is generally bigger near the edge of the parenchyma and becomes smaller toward the inner part near the vessels in every species. The multilayer structure of fibres is visible in the microscope observation and is shown in Fig. 4 where the sclerenchymatic tissue for the six bamboo species is compared.

No differences were found for the average *Arundo donax* fibre, which follows the same trend explained for bamboo species.

Parenchymatic cells: dimensions and shape

Parenchyma cells are located mainly in the inner part of the culm wall and gradually decrease toward the external one. A little band of parenchymal cells divides the last sequence of fibre bundles from the external skin. No substantial differences were found in the parenchymatic tissue for all six species, as reported in Table 5.

Cell size varies greatly: smaller cells are found between fibre bundles or in the external band. However, very different dimensions of parenchymatic cells were found in the

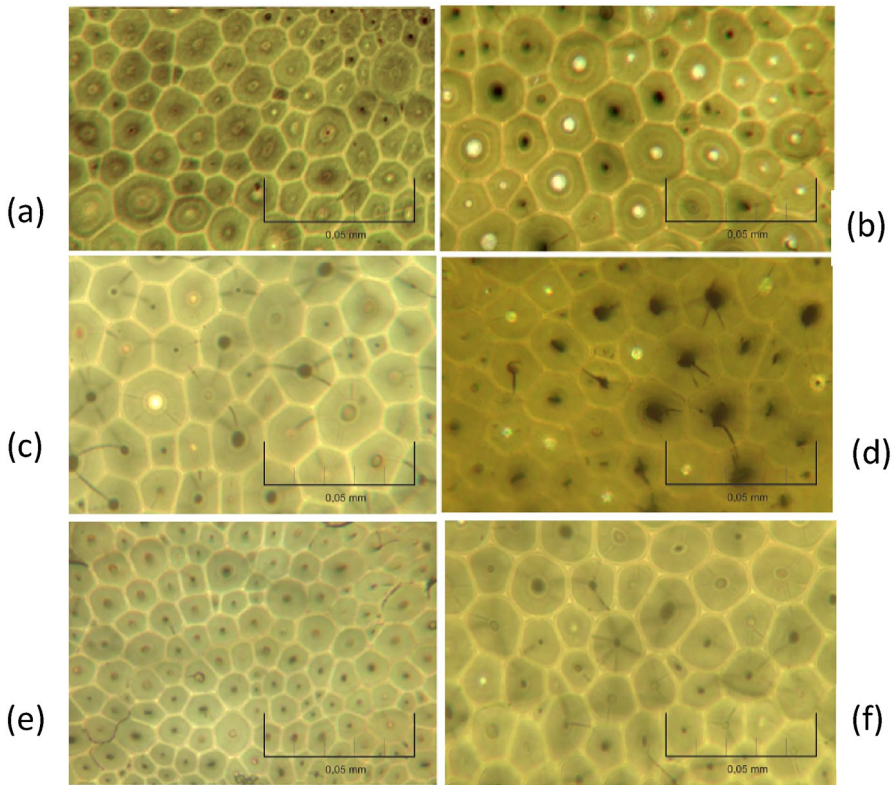
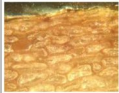


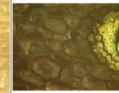
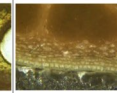
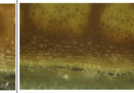
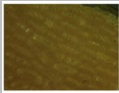
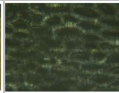
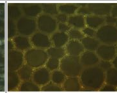
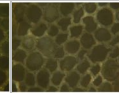

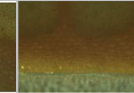
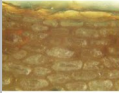
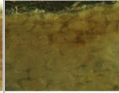
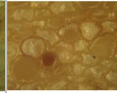
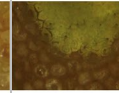
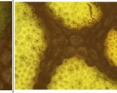
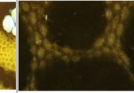
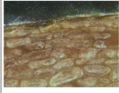

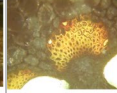
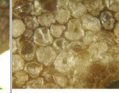
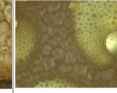
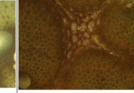


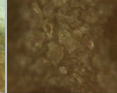
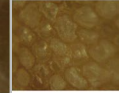
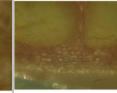
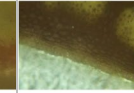
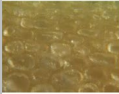
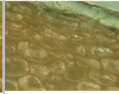
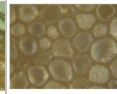
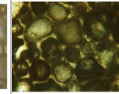
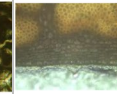
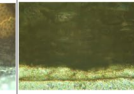
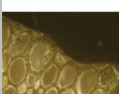
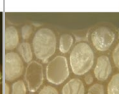
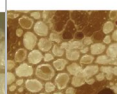
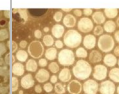
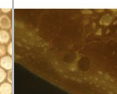
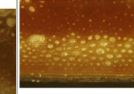


Fig. 4 Sclerenchymatic tissue from the external side of the culm wall of *P.* **a** *edulis*, **b** *bambusoides*, **c** *viridiglaucescens*, **d** *vivax*, **e** *violacescens*, **f** *iridescens*. Transmission optical microscope, 25 \times enlargement

Table 5 A small portion of parenchyma taken from the inner, middle and outer part of each species, for part A and part B of each culm

	INNER		MIDDLE		OUTER	
	Part A	Part B	Part A	Part B	Part A	Part B
<i>P. bambusoides</i>						
<i>P. edulis</i>						
<i>P. iridescens</i>						
<i>P. violacescens</i>						
<i>P. vivax</i>						
<i>P. viridiglaucenscens</i>						
<i>Arundo donax</i>						

Transmission optical microscope, enlargement 25 ×

same part of the section. The morphology of these cells made it difficult to observe them with the optical transmission microscope. As they are short and “cube-like” (Grosser and Liese 1971) cells, the lower light of the microscope cannot go across the section, and the results are dark. However, they were observed with an optical reflection microscope or, in some cases, with a mixed technique to enlighten sclerenchymatic tissue too.

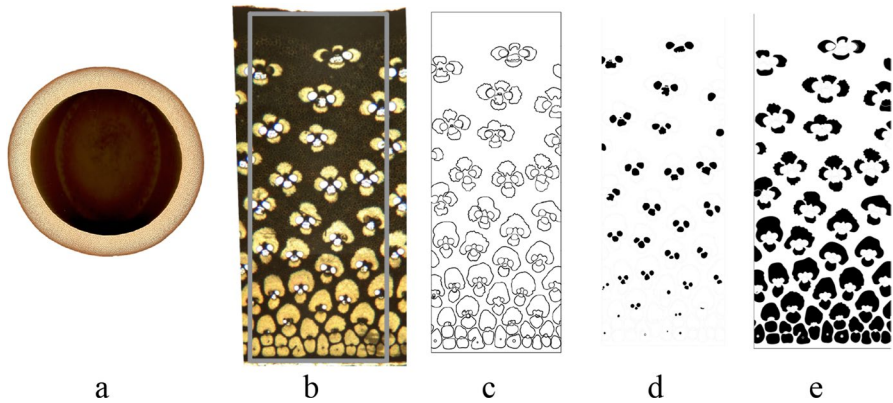


Fig. 5 Image processing from the top part of *P. edulis*: a portion was selected from the culm section (a), and then an image was obtained with a transmission microscope (b). A vectorial image (c) was then obtained with Autocad and divided into fibres (d) and voids (e) with the use of Gimp

Amount and distribution of the components

Images from the microscope were then processed to evaluate the percentage of fibres, parenchyma, and voids, as shown in Fig. 5. Firstly, a portion of the section was chosen to identify a representative and approximately rectangular section. Then, the features in this rectangle were redrawn with splines using CAD software (Autocad 2023, from Autodesk). Next, the presence of each component was analysed by highlighting it with the help of the contrast between black and white.

The mean area percentage of each bamboo component is reported in Table 6. No great differences were found between parts A and B for both fibre and voids. However, part A showed higher fibre percentages, ranging from 0.78% to 20.5%, compared to part B, across all species except *P. viridiglaucescens*. Generally, the fibre content was around 30%. *P. bambusoides*, *P. viridiglaucescens*, *P. vivax*, and *P.*

Table 6 The mean area percentage of each bamboo component for the analysed species from parts A (2.5–3.5 m above the ground) and B (0.5–1.5 m above the ground)

	Part A			Part B		
	Fibre (%)	Voids (%)	Parenchyma (%)	Fibre (%)	Voids (%)	Parenchyma (%)
<i>P. bambusoides</i>	38.8	4.5	56.7	38.5	4.7	56.8
<i>P. edulis</i>	29.4	5.0	65.7	27.0	3.9	69.1
<i>P. iridescens</i>	37.6	6.9	55.5	31.2	5.0	63.8
<i>P. violacescens</i>	27.9	5.8	66.2	26.3	6.5	67.2
<i>P. vivax</i>	38.8	6.1	55.1	33.3	4.7	62.0
<i>P. viridiglaucescens</i>	33.3	4.6	62.1	38.1	4.9	57.0
<i>Arundo donax</i>	17.0	8.7	74.3	15.6	6.0	78.5

iridescens species exhibited fibre contents higher than *P. edulis* and *P. violacescens* species. The percentage of voids ranged from 4 to 7% for both parts A and B in each bamboo species.

Arundo donax exhibited a fibre area percentage under 20%, which is approximately half of that in bamboo. In contrast, it displays a higher void area percentage, which is about 160% of that in bamboo.

The fibre percentage is similar, or in some cases slightly lower, than those reported in the literature for other species. For example, Krause et al. (2016) reported 37.66% for *Dendrocalamus giganteus*, Jiang (2016) found 32.2% for *Phyllostachys glauca*, Seixas et al. (2022) reported a range of 36 to 44% for a *Phyllostachys aurea*, and Londoño et al. (2023) documented 40% for *Guadua angustifolia*.

Regarding the percentage of voids, the results for our *P.* species appear to be slightly lower than those reported in the literature for other species, such as 9.2% for *Dendrocalamus giganteus* (Krause et al. 2016), 8.7% for *Phyllostachys glauca* (Jiang 2016), 9 to 13% for *Phyllostachys aurea* (Seixas et al. 2022), and 9% for *Guadua angustifolia* (Londoño et al. 2023).

The distribution of the components was studied both along the tangential and radial directions. It was found to be relatively constant in the circumferential direction for all six bamboo species and *Arundo donax*, as shown in Fig. 6 for *P. bambusoides* from part A of the culm. In contrast, specific trends were observed along the wall thickness or radial direction. The fibre content within the culm wall increased from the inner part to the outer part. Although all bamboo species showed similar behaviour, the fibre distribution in *Arundo* was relatively constant along the wall thickness and showed a significant peak at the external surface corresponding to the external belt of sclerenchymatic tissue (Fig. 7).

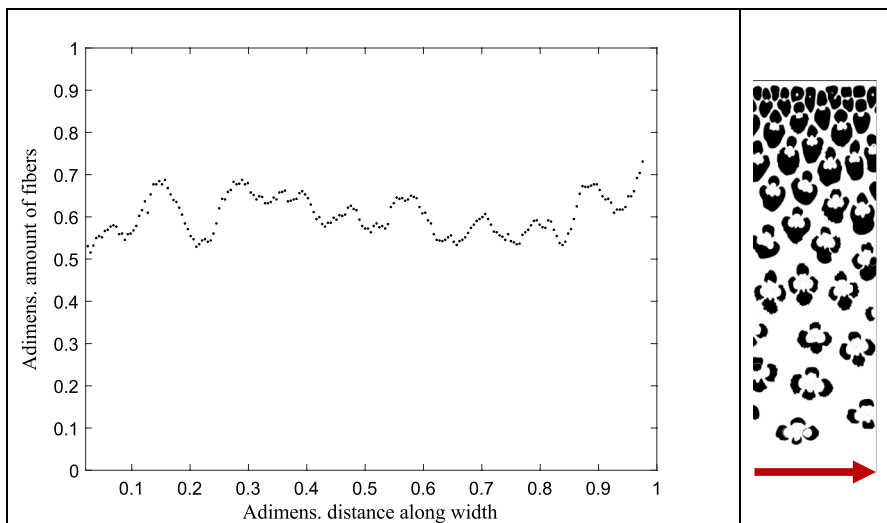


Fig. 6 Distribution of the fibres along the circumferential direction for *P. bambusoides*, from part A of the culm

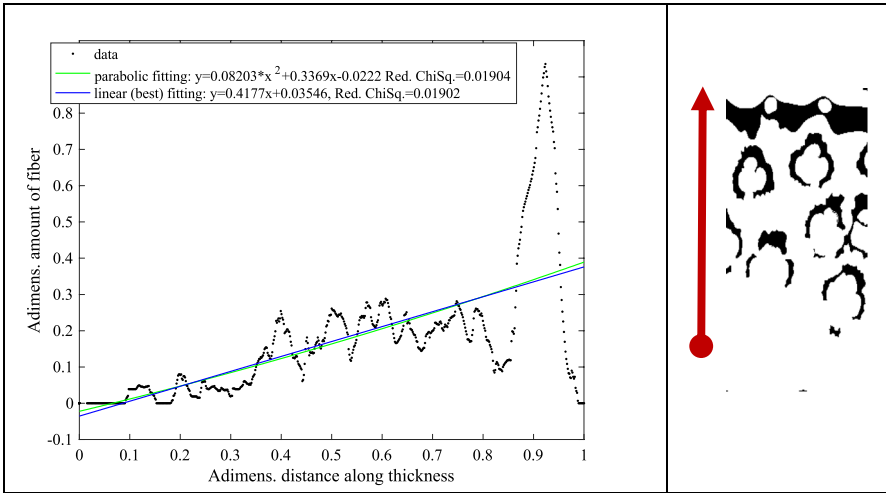


Fig. 7 Distribution of the fibres along the thickness (radial direction) and fitting curves for *Arundo donax* from part A

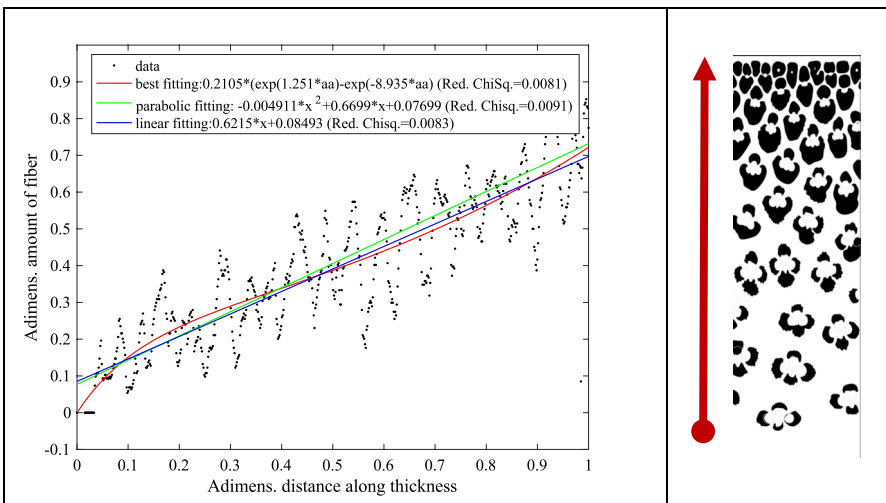


Fig. 8 Distribution of the fibres along the wall thickness or radial direction (black dots) and fitting curves for *P. bambusoides*, from part A of the culm

To identify the most suitable functions for fitting the fibre and void distributions in the radial direction, the Labfit software was employed (Silvia and Silva 1999). The analysis involved testing various types of three-parameter functions, such as exponential, hyperbolic, and linear. For the fibres, the best fit was obtained using exponential and hyperbolic functions. However, both linear and

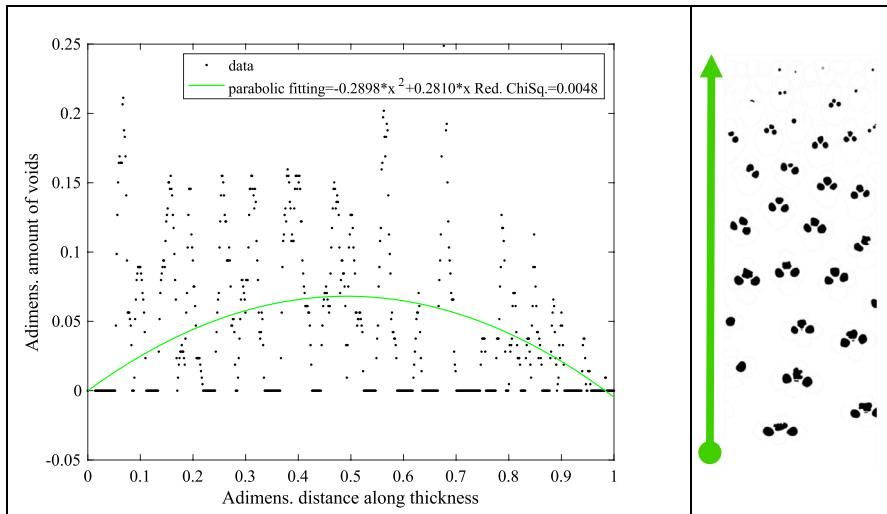


Fig. 9 Distribution of the voids along the thickness and fitting curves for *P. bambusoides*, from part A of the culm

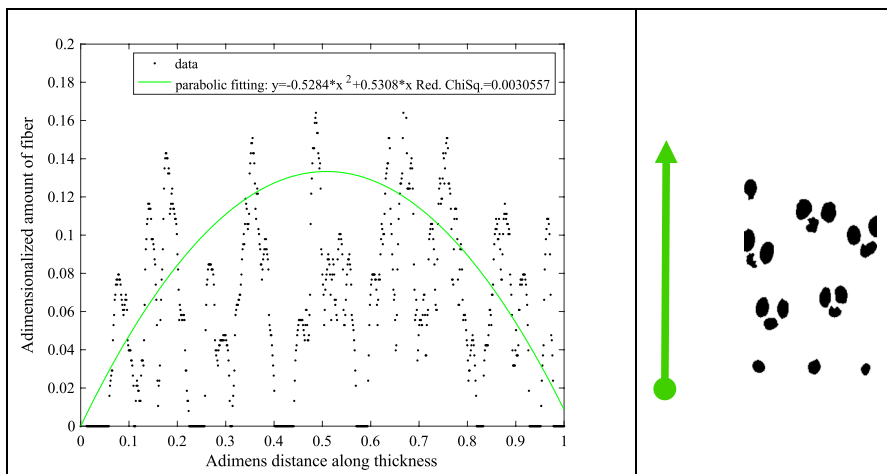


Fig. 10 Distribution of the voids along the thickness and fitting curves for *Arundo donax*, from part A of the culm

parabolic curves showed a relatively good fit for all species, as shown in Fig. 8 for *bambusoides* from part A. The interested reader can find the results for all species in the Electronic Supplementary Material. A trend was also recognized in the distribution of voids. The analysis with LabFit showed that the parabolic functions provided the best fit as reported in Fig. 9 for *P. bambusoides* part A, and in Fig. 10 for *Arundo donax* part A.

Discussion about the relation between microscopic features and mechanical properties

As established in the literature (Grosser and Liese 1971), the distribution of the fibres and the arrangement in the microfibril (Kanzawa et al. 2011) impact the strength and stiffness of the culm (Shao et al. 2010).

To test correlations, we consider the mechanical properties of previous research for the studied species; in particular, reference is made to tensile tests (Molari et al. 2020; Greco et al. 2019).

Figure 11 shows the setup of the tests. The tensile stress considered is the force divided by the average area. The stress has a relatively good linear correlation ($R^2 > 0.7$) with the fibre content, as shown in Fig. 12a, where each point represents the tensile stress of each culm and the square depicts the average. The data are for the A and B parts of the culm. For the linear regression, Fig. 12b shows the residuals of the data that suggest that the tension strength is mainly related to fibre percentage.

We further explore the relationship between the microscopical features and the macroscopical characteristics of the material. To accomplish this, we employed the Rule of Mixtures (RoM) to estimate the longitudinal elasticity modulus and strength of each species. Next, we compared these estimates with the results obtained from actual tests published in the literature.

The effective longitudinal modulus of elasticity was estimated with the fibre percentage, measured in this study, and the modulus of elasticity of each component. In particular, assuming the values of 40 GPa and 55 GPa for the longitudinal modulus of elasticity for the fibres, E_f , and 1.9 GPa and 2 GPa as the longitudinal modulus of elasticity for the matrix, E_m (Dixon and Gibson 2014; Nogata and Takahashi 1995) respectively), the effective Young's modulus E_1 of the culm was calculated as,

$$E_1 = fE_f + (1 - f - \nu)E_m \quad (1)$$

Fig. 11 Set up of the tensile test



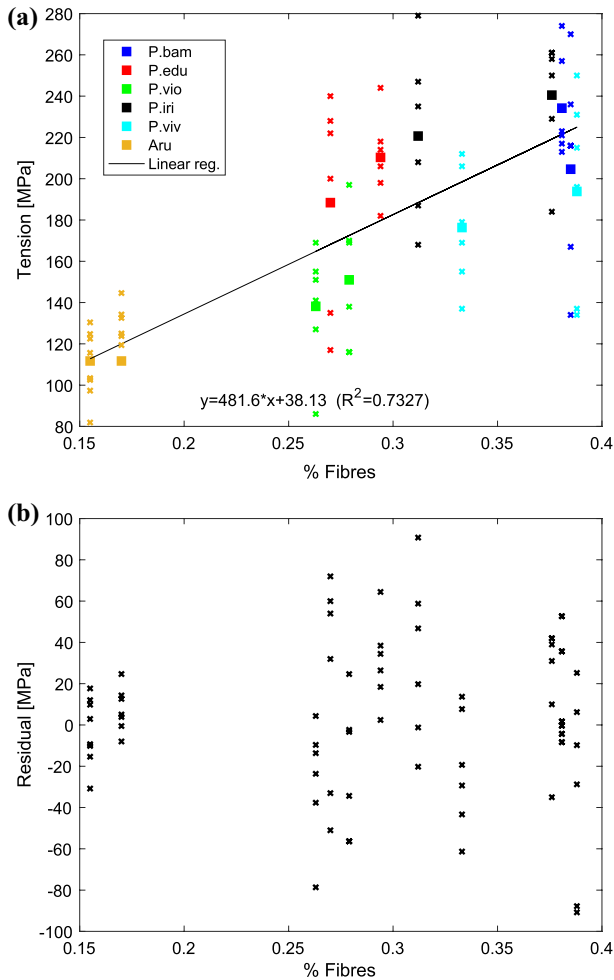


Fig. 12 **a** Tension strength in the longitudinal directions versus fibre area percentage. Samples of parts A and B are included for each species, **b** Residuals of the data for the linear regression

where f is the ratio of fibre area over the total area and v is the ratio of void over the total area.

The comparison with the experimental data reported for each species (Table 7, Fig. 13) from Molari et al. (2020), and Greco et al. (2019) shows similar values, especially for *P. viridiglaucescens*, *P. iridescens* and *P. edulis* species, while some differences can be observed for *P. bambusoides*, *P. violaceus*, and *P. vivax* species.

To predict the failure of each species using the results of this study, the following analysis was accomplished. In the initial zone, when both the matrix and the fibres are in the elastic range, each constituent contributes to supporting the external load according to its stiffness. For the axial case, the stiffness is equal to

Table 7 Comparison between experimental modulus of elasticity in the longitudinal direction E_1 obtained with the use of the rule of mixture (RoM E_1) and from tension test results (Exp. E_1)

Species	Culm part	% Fibres	Young's modulus E_1 (GPa)	
			RoM (Dixon and Gibson 2014/ Nogata and Takahashi 1995)	Exp. Avrg (CoV)
<i>P. bambusoides</i>	A	38.8	16.6/22.5	21.09 (0.11)
	B	38.5	16.5/22.3	16.91 (0.04)
<i>P. edulis</i>	A	29.4	13.0/17.5	17.04 (0.07)
	B	27.0	12.1/16.2	14.21 (0.06)
<i>P. violacescens</i>	A	27.9	12.4/16.7	17.34 (0.19)
	B	26.3	11.8/15.8	19.16 (0.31)
<i>P. viridiglaucescens</i>	A	33.3	14.5/19.6	18.82 (0.15)*
	B	38.1	16.3/22.1	
<i>P. iridescens</i>	A	37.6	16.1/21.8	19.79 (0.19)
	B	31.2	13.7/18.4	16.19 (0.09)
<i>P. vivax</i>	A	38.8	16.6/22.4	16.58 (0.19)
	B	33.3	14.5/19.6	15.35 (0.16)

CoV is the ratio of the standard deviation over the mean

*For *v. iridiglaucescens* the data do not take into account the position of the specimens in the culm

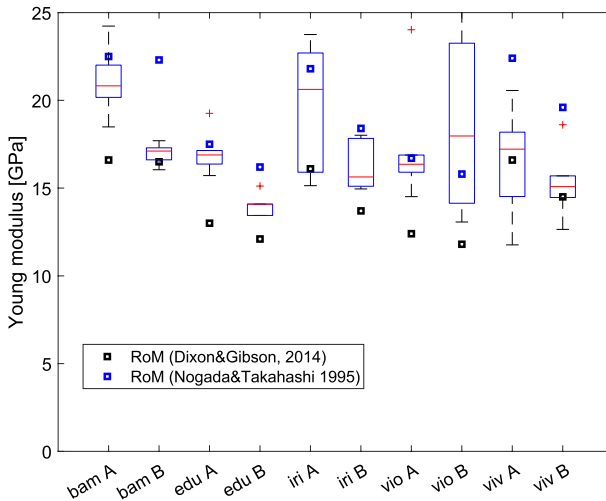


Fig. 13 Comparison between the experimental modulus of elasticity in the longitudinal direction and that obtained with the rule of mixture considering the modulus of elasticity of fibers and matrix calculated by Nogata and Takahashi (1995) and by Dixon and Gibson (2014)

the product of the modulus of elasticity times the area over the length. Thus, the total force F in the composite can be calculated as,

$$F = \left(\frac{E_f A_f}{L} + \frac{E_m A_m}{L} \right) \Delta, \quad (2)$$

where Δ is the elongation of the specimen. By dividing over the area A of the whole composite, the effective stress σ_1 is equal to

$$\sigma_1 = E_f f \varepsilon + E_m (1 - f - v) \varepsilon \quad (3)$$

where ε is the strain, which is equal to Δ over the length. In terms of the stress in the fibres, i.e. $E_f \varepsilon$, the effective stress can be calculated as,

$$\sigma_1 = E_f \varepsilon \left[f + E_m \frac{(1 - f - v)}{E_f} \right] \quad (4)$$

The composite fails in a brittle mode when the stress in the fibres reaches its limit, as the matrix cannot support all the external load. Considering the fibre strength of $\sigma_f = 610$ MPa (Amada et al 1996), the strength of each species was calculated and plotted against that measured in tests, as presented in Table 8 and Fig. 14. In some cases, good predictions are observed. The percentage differences between the estimates with respect to the measured value range from 0.17% and 26.2%. Differences may be attributed to many factors, mainly variations in the

Table 8 Comparison of the longitudinal tensile strength calculated as a result of the experimental tensile test (σ_{MAX}) from Greco et al. (2019) and Molari et al. (2020), and with the use of Eq. (4) considering the elastic moduli reported by Dixon and Gibson (2014) and Nogata and Takahashi (1995)

Species	Culm part	σ_{MAX} (MPa)		
		Experimental Mean (CoV)	Dixon and Gibson (2014)	Nogata and Takahashi (1995)
<i>P. bambusoides</i>	A	234 (0.11)	249	245
	B	205 (0.26)	247	243
<i>P. edulis</i>	A	210 (0.10)	195	191
	B	188 (0.31)	182	177
<i>P. violacescens</i>	A	151 (0.22)	186	182
	B	138 (0.21)	177	172
<i>P. viridiglaucescens</i>	A	214 (0.12)*	217	213
	B		245	241
<i>P. iridescens</i>	A	241 (0.12)	241	238
	B	221 (0.18)	205	201
<i>P. vivax</i>	A	194 (0.25)	249	245
	B	176 (0.16)	217	213

*For *P. viridiglaucescens* the data do not take into account the position of the specimens in the culm

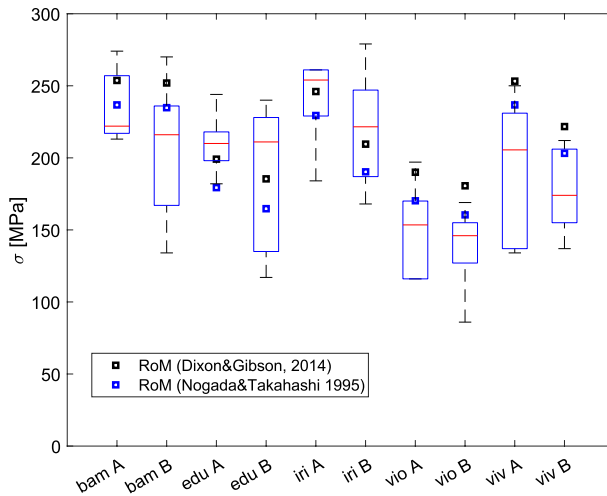


Fig. 14 Comparison between the experimental maximum stress and that obtained with the rule of mixture considering the modulus of elasticity of fibers and matrix calculated by Nogata and Takahashi (1995) and by Dixon and Gibson (2014)

mechanical parameters of each species with respect to the values assumed in this study.

Regarding the circumferential direction, the RoM is not able to catch the real behaviour of the composite bamboo material, as pointed out by Akinbade and Harries (2021), even including the correction of Halpin–Tsai. In the circumferential direction, a crucial role is played by the voids, as they create stress concentrations.

Considering the results shown in the previous section, depicting more voids in the central part of the culm wall, it may be argued that the weakest part of the culm wall concerning circumferential stress is the center of the culm wall.

This appears to explain the variation of the circumferential strength along the thickness obtained by Akinbade et al. (2019) where the circumferential strength along the thickness has a parabolic shape with its smallest values in the inner part.

However, the behaviour of the bamboo composite material in the transversal direction is much more complex and needs further investigation (Greco et al. 2022).

Conclusion

Bamboo is emerging as a sustainable construction material, but its adoption is hindered by a lack of knowledge about its diverse species. This paper presents a comprehensive analysis of six *Phyllostachys* bamboo species and *Arundo donax* grown in Italy. By combining microscopic examination of their key components with evaluations of distribution, quantity, and mechanical behavior, this study offers valuable insights to support academics, professionals, and new businesses in the sustainable utilization of local bamboo and other temperate plants. However, the limited number of culms collected from different locations may

affect the representativeness of the results due to site-specific and natural variations among individuals. Despite these limitations, some conclusions can still be drawn.

Analysis using polarized optical microscopy focused on the shape and size of vascular bundles, sclerenchymatic cells, and parenchymatic cells in bamboo stem cross-sections. Bamboo vascular bundles have four small fiber islands inside, stretching towards the outside with two large fiber islands. In *Arundo donax*, a ring of sclerenchymatous tissue surrounds the vessels, and the part around the phloematic vessels is thicker.

Vascular bundles are smaller at the top of the culm than at the bottom, *P. viol-ascens* bamboo species and *Arundo donax* have smaller vascular bundle dimensions, and fiber dimensions vary by position along the culm and within the culm wall. The average fiber diameter ranges from 12 to 20 μm (inner) to 15–22 μm (outer), with a nearly constant ratio between cell size and wall thickness. No significant differences were found in parenchymatic tissue. The fiber cell dimensions of the *P.* species analyzed are similar to those grown in tropical and subtropical climates. but more data is needed.

Imagine techniques were applied to investigate the composition of the cross section. The average value of fibre volume fraction ranges from 27.9 to 38.8% for the A part and from 26.3 to 38.5% for the B part of the culms. The void volume fraction goes from 4.5 to 6.9% for the A part and from 3.9 to 6.5% for the B part of the culms. In the case of *Arundo donax*, the average value of fibre volume fraction is sensibly lower and corresponds to 17% for the A part and 15.56 for the B part, while the average value of the vessel volume fraction corresponds to 8.66% for the A part and 5.99 for the B part.

The distribution of the components was studied along the thickness (radial direction) and along the culm wall (circumferential direction). Fibre content increases from the inner to the outer part of the culm wall, fitting well with linear and parabolic functions for all bamboo species. Bamboo species showed similar behaviour, while the fibre distribution in *Arundo* was relatively constant along the wall thickness, with a significant peak at the external surface due to the sclerenchymatic tissue. Void distribution followed a parabolic function with null values at the inner and outer surfaces.

The amount of fibre and voids was related to the mechanical properties. Longitudinal tension can be predicted by the Rule of Mixture, but this model falls short in the transversal direction. The distributions of the components deeply influence strength and stiffness. A crucial role is played by the voids.

Supplementary Information The online version contains supplementary material available at <https://doi.org/10.1007/s00226-024-01547-0>.

Acknowledgements The authors thank Prof. Annalisa Tassoni for sharing her knowledge in vegetal biology and Dr. Daniele Moro for the support in using the microscope.

Author contributions Conceptualization: SG LM JGG GV Writing the main manuscript text: SG LM JGG Data elaboration and preparation of graphs and pictures: SG LM Optical microscope analysis: GV Reviewing and editing the manuscript: SG LM JGG GV

Funding Open access funding provided by Alma Mater Studiorum - Università di Bologna within the CRUI-CARE Agreement.

Declarations

Conflict of interest The authors declare that they have no conflict of interest.

Open Access This article is licensed under a Creative Commons Attribution 4.0 International License, which permits use, sharing, adaptation, distribution and reproduction in any medium or format, as long as you give appropriate credit to the original author(s) and the source, provide a link to the Creative Commons licence, and indicate if changes were made. The images or other third party material in this article are included in the article's Creative Commons licence, unless indicated otherwise in a credit line to the material. If material is not included in the article's Creative Commons licence and your intended use is not permitted by statutory regulation or exceeds the permitted use, you will need to obtain permission directly from the copyright holder. To view a copy of this licence, visit <http://creativecommons.org/licenses/by/4.0/>.

References

- Akinbade Y, Harries KA (2021) Is the rule of mixture appropriate for assessing bamboo material properties? *Constr Build Mater*. <https://doi.org/10.1016/j.conbuildmat.2020.120955>
- Akinbade Y, Harries KA, Flower CV, Nettleship I, Papadopoulos C, Platt S (2019) Through-culm wall mechanical behaviour of bamboo. *Constr Build Mater* 216:485–495. <https://doi.org/10.1016/j.conbuildmat.2019.04.2140950-0618/>
- Amada S, Munekata T, Nagase Y, Ichikawa Y, Kirigai A, Zhifei Y (1996) The mechanical structures of bamboos in viewpoint of functionally graded and composite material. *J Compos Mater* 30(7):800–819. <https://doi.org/10.1177/002199839603000703>
- Amada S, Ichikawa Y, Munekata T, Nagase Y, Shimuzu H (1997) Fiber texture and mechanical graded structure of bamboo. *Compos Part B*. [https://doi.org/10.1016/S1359-8368\(96\)00020-0](https://doi.org/10.1016/S1359-8368(96)00020-0)
- Conte P, Fiore V, Valenza A (2018) Structural and mechanical modification induced by water content in giant wild reed (*A. donax* L.). *ACS Omega* 3(12):18510–18517. <https://doi.org/10.1021/acsomega.8b02649>
- Dai F, Wang Z, Wang H, Zhang W, Zhong T, Tian G (2023) Vascular bundle characteristics and mechanical properties of *Dendrocalamus sinicus*. *Constr Build Mater*. <https://doi.org/10.1016/j.conbuildmat.2022.129858>
- Dessalegn Y, Singh B (2019) Effect of analysis on morphology of bamboo fibre: a review. *Int J Eng Sci Res Technol*. Retrieved from ISSN: 2277-9655
- Dixon PG, Gibson LJ (2014) The structure and mechanics of Moso bamboo material. *J R Soc Interface* 11:20140321. <https://doi.org/10.1098/rsif.2014.0321>
- Fangchun Z (1981) Studies on physical and mechanical properties of bamboo wood. *J Nanjing Technol*. <https://doi.org/10.3969/j.jssn.1000-2006.1981.02.001>
- Greco S, Molari L, Maraldi M (2019) Assessing the mechanical properties of bamboo cultivated in Italy. In: 18th international conference on non-conventional materials and technologies (NOCMAT 2019). Nairobi, Kenya
- Greco S, Molari L, Valdrè G, Garcia JJ (2022) Finite element analysis for the prediction of the circumferential bamboo strength. In: 18th International conference on non-conventional materials and technologies (NOCMAT 2022). <https://doi.org/10.5281/zenodo.6811560>
- Greco S, Maraldi M, Molari L (2023) Grading bamboo through four-point bending tests. A report on six species of Italian bamboo. *Constr Build Mater* 404:133168. <https://doi.org/10.1016/j.conbuildmat.2023.133168>
- Gritsch CS, Kleist G, Murphy RJ (2004) Developmental changes in cell wall structure of phloem fibres of the bamboo *Dendrocalamus asper*. *Ann Bot* 94:497–505. <https://doi.org/10.1093/aob/mch169>
- Grosser D, Liese W (1971) On the anatomy of Asian bamboos, with special reference to their vascular bundles. *Wood Sci Technol* 5:290–312. <https://doi.org/10.1007/BF00365061>

- Hardion L, Verlaque R, Saltonstall K, Leriche A, Vila B (2014) Origin of the invasive *Arundo donax* (Poaceae): a trans-Asian expedition in herbaria. *Ann Bot* 114(3):455–462. <https://doi.org/10.1093/aob/mcu143>
- Hartono R, Purba FVA, Iswanto AH, Priadi T, Sutiawan J (2022) Fiber quality of yellow bamboo (*Bambusa vulgaris* vitata) from Forest area with special purpose Pondok Buluh, Simalungun Regency, North Sumatera Province. *IOP Conf Ser Earth Environ Sci* 1115:012084. <https://doi.org/10.1088/1755-1315/1115/1/012084>
- Janssen J (1991) Mechanical properties of bamboo. Kluwer Academic Publishers, Dordrecht
- Kanzawa E, Aoyagi S, Nakano T (2011) Vascular bundle shape in cross-section and relaxation properties of Moso bamboo (*Phyllostachys pubescens*). *Mater Sci Eng C* 31:1050–1054. <https://doi.org/10.1016/j.msec.2011.03.004>
- Khantayanuwong S, Yimlamai P, Chitbanyong K, Wanitpinyo K, Pisutpiched S, Sugkaew S, Sukyai P, Puangsin B (2023) Fiber morphology, chemical composition, and properties of kraft pulping hand-sheet made from four Thailand bamboo species. *J Nat Fiber*. <https://doi.org/10.1080/15440478.2022.2150924>
- Krause JQ, Silva FD, Ghavami K, Gomes OD, Filho RD (2016) On the influence of *Dendrocalamus giganteus* bamboo microstructure on its mechanical behavior. *Constr Build Mater* 127:199–209. <https://doi.org/10.1016/j.conbuildmat.2016.09.104>
- Li X, Shupe TF, Peter G, Hse C-Y, Eberhardt T (2007) Chemical changes with maturation of the bamboo species *Phyllostachys pubescens*. *J Trop For Sci* 19(1):6–12
- Liese W, Köhl M (2015) Bamboo, the plant and its uses. Tropical Forestry, Hamburg
- Liese W, Schmitt U (2006) Development and structure of the terminal layer in bamboo culms. *Wood Sci Technol* 40:4–15. <https://doi.org/10.1007/s00226-005-0046-5>
- Liu D, Song J, Anderson DP, Chang PR, Hua Y (2012) Bamboo fiber and its reinforced composites: structure and properties. *Cellulose* 19:1449–1480. <https://doi.org/10.1007/s10570-012-9741-1>
- Molari L, García JJ (2021) On the radial variation of the transverse mechanical properties of bamboo. *J Build Eng*. <https://doi.org/10.1016/j.jobbe.2020.101557>
- Molari L, Coppolino FS, García JJ (2021) *Arundo donax*: A widespread plant with great potential as sustainable structural material. *Constr Build Mater* 268:121143. <https://doi.org/10.1016/j.conbuildmat.2020.121143>
- Molari L, Mentrasti L, Fabiani M (2020) Mechanical characterization of five species of Italian bamboo. *Structures*. <https://doi.org/10.1016/j.istruc.2019.12.022>
- Murphy RL, Alvin KL (1997) Fibre maturation in the bamboo *Gigantochloa scortechinii*. *IAWA J* 18:147–156. <https://doi.org/10.1163/22941932-90001476>
- Nogata T, Takahashi H (1995) Intelligent functionally graded material: bamboo. *Compos Eng* 5:743–751. [https://doi.org/10.1016/0961-9526\(95\)00037-N](https://doi.org/10.1016/0961-9526(95)00037-N)
- Parameswaran N, Liese W (1976) On the fine structure of bamboo fibres. *Wood Sci Technol* 10:231–246. <https://doi.org/10.1007/BF00350830>
- Rüggeberg M, Burgert I, Speck T (2010) Structural and mechanical design of tissue interfaces in the giant reed *Arundo donax*. *J R Soc Interface* 7:499–506. <https://doi.org/10.1098/rsif.2009.0273>
- Shao Z-P, Fang C-H, Huang S-X, Tian G-L (2010) Tensile properties of Moso bamboo (*Phyllostachys pubescens*) and its components with respect to its fiber-reinforced composite structure. *Wood Sci Technol* 44:655–666. <https://doi.org/10.1007/s00226-009-0290-1>
- Silva WP, Silva CMDPS (1999–2023) LAB fit curve fitting software (nonlinear regression and treatment of data program) V 7.2.50c, online. Available from world wide web: www.labfit.net, date of access: Year-Month-Day
- Spatz H-C, Beismann H, Bruchert F, Emanns A, Speck T (1997) Biomechanics of the giant reed *Arundo donax*. *Philos Trans R Soc Lond* 357:1–10. <https://doi.org/10.1098/rstb.1997.0001>
- Trujillo L (2016) Bamboo material characterisation. In: K Harries, B Sharma (eds) *Nonconventional and vernacular construction materials*, pp. 365–392
- Wahab R, Mustafa MT, Rahman S, Salam MA, Sulaiman O, Sudin M, Rasat MS (2012) Relationship between physical, anatomical and strength properties of 3-year-old cultivated tropical bamboo. *ARPN J Agric Biol Sci* 7(10):782–791
- Wang X, Ren H, Zhang B, Fei B, Burgert I (2012) Cell wall structure and formation of maturing fibres of moso bamboo (*Phyllostachys pubescens*) increase buckling resistance. *R Soc Interface* 9:988–996. <https://doi.org/10.1098/rsif.2011.0462>

Wang F, Shao Z, Wu Y (2013) Mode II interlaminar fracture properties of Moso bamboo. *Compos B Eng* 44(1):242–247. <https://doi.org/10.1016/j.compositesb.2012.05.035>

Zea EE, Habert G (2014) Environmental impacts of bamboo-based construction materials representing global production diversity. *J Clean Prod* 69:117–127. <https://doi.org/10.1016/j.jclepro.2014.01.067>

Publisher's Note Springer Nature remains neutral with regard to jurisdictional claims in published maps and institutional affiliations.